MECHANICAL INSTABILITY OF NiTi IN TENSION, COMPRESSION AND SHEAR

D. FAVIER[1], Y. LIU[2], L. ORGEAS[1], G. RIO[3]

[1] *Laboratoire Sols, Solides Structures, CNRS-Université Joseph Fourier-Ins. Nat. Polytechnique, B.P.53, 38041 Grenoble Cedex 9, France*

[2] *Department of Mechanical and Materials Engineering, University of Western Australia, Crawley, WA 6009, Australia*

[3] *Laboratoire de Génie Mécanique et Matériaux, Université de Bretagne Sud, 2 Rue le Coat Saint Haouens, 56325 Lorient, France*

1. Introduction

Shape memory alloys (SMAs) are known to exhibit a range of novel thermomechanical properties due to thermoelastic martensitic transformations. The superelasticity is a quasi-elastic deformation far beyond the conventional elastic limit of the material when deformed at certain temperatures above A_f, the finishing temperature of the reverse martensite-to-austenite transformation. This phenomenon is associated with stress-induced martensitic (SIM) transformation. If the temperature is lowered to below M_f, the finishing temperature of the forward austenite-to-martensite transformation, the deformation proceeds by martensite reorientation. Martensite may deform by reorientation forth and back with alternating stresses in opposite directions. This deformation mode is known as the ferroelasticity, in recognition of its phenomenological similarity to ferromagnetism.

Numerous experimental works have been performed in the past three decades aiming at characterising the thermo-mechanical behaviour of SMAs in order to provide experimental evidences for the establishment of constitutive models. These studies have been devoted to both single-crystal and polycrystal specimens, mainly using Cu-based and NiTi SMAs. Most mechanical testing has been carried out in tension using wire or strip specimens.

Superelastic tensile tests in most of NiTi alloys exhibit Lüders type engineering stress plateau with an upper yield stress during loading and an inverse stress peak during unloading. This localised deformation has been studied by *in-situ* optical observations [1] and more recently by *in-situ* full-field temperature monitoring and by local deformation measurement using multiple miniature extensometers [2,3]. Shaw and Kyriakides have proposed to approximate the NiTi behaviour as that of a finitely deforming elasto-plastic solid with a trilinear up-down-up nominal stress-strain response [4]. Two models have been tested. The first one considered that the true stress-logarithmic strain behaviour was always rising although the nominal stress-strain curves

of the intermediate branch had a negative slope. The middle branch of the true stress-strain response for the second model had a negative slope. The two models have been implemented in a finite element code in order to simulate experimental inhomogeneous tensile tests [4] neglecting the thermo-mechanical coupling of the tensile sample with its environment. For the two models, Lüders-like tensile behaviour was well simulated, at least qualitatively. However, for the first model, the localisation was interpreted more as a geometrical instability than a material instability. In the second model, the onset and the propagation of the localised deformation was interpreted as being associated with nucleation and propagation of martensitic transformation. Shaw et al rejected the first model arguing that the second model seemed to better fit experimental data than the first one. Their conclusions did not take into account (1) thermomechanical coupling, known to have a strong influence on the localisation [5,6], and (2) experimental results obtained under other stress conditions than tension. Thermo-mechanical coupling has been later studied by Shaw [7], but only for the second scheme.

This paper presents experimental results, physical arguments and numerical simulation aiming to clarify the instability phenomena observed for NiTi polycrystalline alloys. In the first part, experimental results on an equiatomic NiTi involving tension and other stress states are presented. The second part offers a discussion of the nucleation-propagation hypothesis for the instability from a metallurgical perspective. The last part presents numerical simulation of tension, compression and shear tests.

2. Experimental Results in Tension, Compression and Shear of NiTi

A commercial polycrystalline equiatomic NiTi alloy was used. As-received 3.2 mm and 1.3 mm thick sheets were homogenized at 1173 K for 3.6 ks, cold-rolled with a 18 % thickness reduction and annealed at 703 K for 1.8 ks. After such treatments, the material showed a two-step A→R→M transformation on cooling ($R_s \approx 321$ K, $R_f \approx 308$ K, $M_s \approx 283$ K, $M_f \approx 226$ K) and a one-step transformation M→A on heating ($A_s \approx 301$ K, $A_f \approx 328$ K).

Specimens for tension-compression tests were bone-shaped specimens with a deformation gauge section of 40 mm in length, 5.6 mm in width and 2.7 mm in thickness [8]. To enable compressive loading on such specimens, a specially designed anti-buckling gripping system was designed. Specimens for shear tests were rectangular in shape with a shear gauge section of $30 \times 3 \times 1.05$ mm^3. Isothermal testing conditions were achieved using an oil bath for temperature control with an accuracy of ± 1 K. Deformation was carried out using a slow strain rate of 10^{-3} s^{-1} for tension-compression and $1.75\ 10^{-3}$ s^{-1} for shear. For tension-compression tests, both local strain (ε %, LM) and global strain (ε %, GM) were measured. LM was measured using an extensometer of a 10 mm gauge length that was mounted on the specimen in the oil bath, whereas GM was calculated from the total length variation of the specimen [9]. The shear strain γ was calculated from the measurement of the relative displacement of the mobile grip of the shear testing apparatus with respect to the stationary grip using a local extensometer mounted in the oil bath.

Three tension-compression loops are shown in Figure 1 of the same sample tested at 333, 338 and 343 K sequentially. The stress was estimated as the engineering stress F/S_0

(F and S_0 being respectively the current applied force and the initial cross-section) whereas the strain ε was estimated as the engineering strain $\Delta l/l_0$ (l_0 and Δl being respectively the initial gauge length and its variation). Superelastic behaviour was observed in tension and compression for the three temperatures ($> A_f$). Transformation stresses were higher in compression than in tension. Conversely, transformation strains were higher in tension than in compression. Lüders-like deformation behaviour, as characterized by a distinctive stress plateau on an engineering stress-strain curve, was observed in tension during both the forward and reverse transformations, but not in compression. Two virgin samples were also tested separately in tension and in compression at 333 K, as shown in Figure 2. The occurrence of Lüders-like deformation under the condition of monotonic loading conforms to the observations established for the alternative tension-compression loading conditions. The heterogeneous nature of the Lüders-like deformation is illustrated in Figure 3, where the measurement of the global strain (GM) is plotted as a function of the local strain (LM) for the tensile test shown in Figure 2. The corresponding points on the curves shown in Figures 2 and 3 are labelled identically.

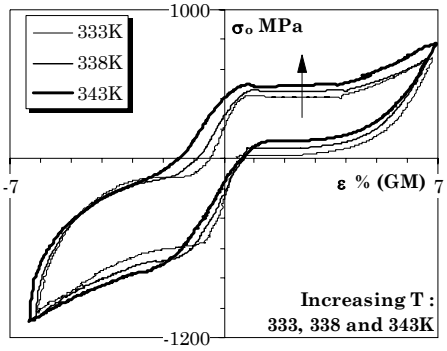

Figure 1: Isothermal tension-compression loops at T = 333, 338 and 343 K.

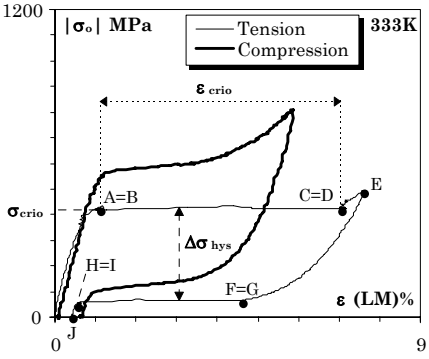

Figure 2: Tension and compression tests on two virgin samples at T = 333 K.

Figure 4 shows a specimen deformed in shear at temperatures above A_f. The stress-strain curves demonstrate that the deformation was well superelastic and that no Lüders-like behaviour occurred.

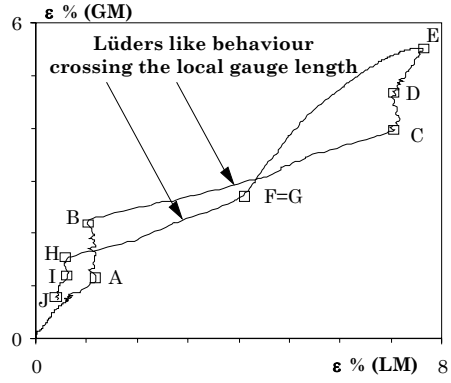

Figure 3: Global strain versus local strain measurement during the tensile test of Fig.2.

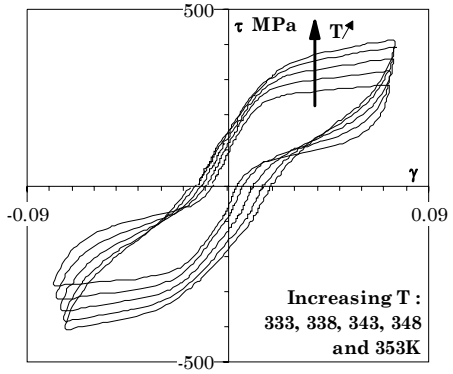

Figure 4: Isothermal shear loops at T = 333, 338, 343, 348 and 353 K.

3. Localised Deformation and Nucleation-propagation Hypothesis

3.1. REMARKS ON LOCALISATION OF DEFORMATION

Figure 5 shows the deformation of a Ti-50.0at%Ni wire specimen in tension via martensite reorientation, as measured by three LM measurements [10]. The three engineering tensile stress-strain curves are characterized by an initial stage of deformation prior to the stress drop at the onset of a stress plateau, which terminated at 6% strain. The localisation of deformation during this Lüders-like behaviour is emphasised by plotting the measurement of the three local strains as a function of the time elapsed during deformation, as shown in Figure 6.

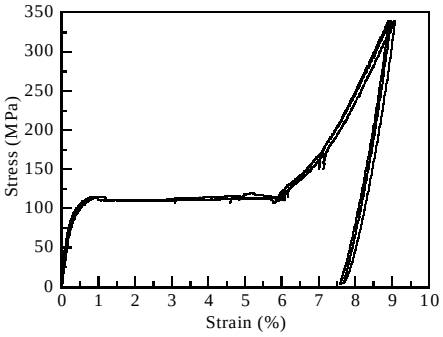

Figure 5: Tension test of martensite in NiTi.

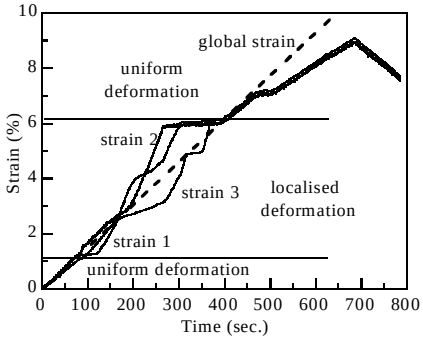

Figure 6: Measurement of local strains as a function of deformation time.

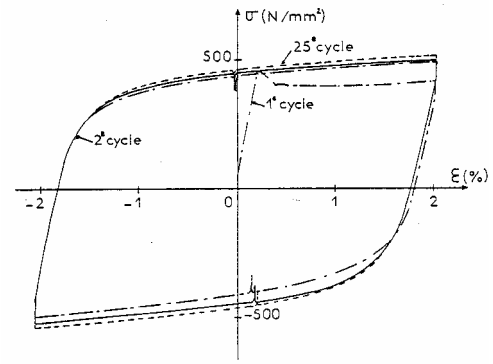

Figure 7: Tension-compression of mild steel.

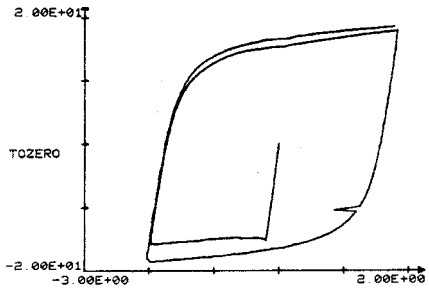

Figure 8: Torsion of mild steel.

It is well-known that Lüders deformation is often observed in mild steel tensile tests, as shown in Figure 7 [11]. For this type of materials, Lüders deformation is observed for other stress states, as seen in Figure 8, which shows a shear stress-strain curve deduced from a torsion test using a thin-tube specimen. It has been suggested that there exist some similarities in macroscopic events during tensile tests between superelastic NiTi alloys and fine-grained steel strips or wires [3]. This suggestion does not seem to prevail for other stress states, as demonstrated in the comparison between shear of NiTi sheets, where no Lüders bands were observed (Figure 4), and torsion of mild steel thin tubes (Figure 8).

3.2. THE NUCLEATION-PROPAGATION HYPOTHESIS

The stress plateau exhibited by NiTi deformed in tension (Figures 2 and 3) has been recognised as being associated with stress-induced martensitic transformation [1]. To explain the mechanical instability of the transformation, the theory postulates that the transformation requires a higher stress for initial nucleation and a lower stress for transformation propagation. This theory justifies the use of constitutive models which acknowledge material instabilities, like the second model used by Shaw et al [4], and which have been extensively used to model instabilities occurring in materials like high-density polyethylene.

However, this postulation for the stress-induced martensitic transformation in NiTi is questionable in several accounts [12]:

(1) Whereas Lüders-like behaviour has been widely observed in NiTi during tensile deformation, there has been no convincing experimental evidence in the literature showing the occurrence of similar deformation behaviour for stress-induced transformation under other deformation modes, where nucleation is also a prerequisite to transformation. Instead, there have been experimental evidences of the absence of Lüders-like behaviour during compression (Fig. 2) or shear (Fig. 4) of samples that show Lüders-like behaviour in tension.
(2) Lüders-like behaviour is also observed during tensile deformation by martensite reorientation, in which no nucleation or phase transformation is involved (Fig. 5).

(3) It has been frequently observed that the mechanical instability may start well beyond 1% of tensile strain deviating from elastic linearity. It has also been well established that recoverable strain continues to increase with deformation beyond the end of the instability [13,14]. These observations suggest that the stress plateau is only a manifestation of localised deformation with no proof to either the start or the finish of the transformation.

(4) From a metallurgical point of view, whereas a deformation wave can propagate across grain boundaries from grain to grain in a polycrystalline matrix, phase transformation cannot propagate across grain boundaries without nucleation in adjacent grains.

These evidences suggest that the mechanical instability of NiTi during tensile deformation be due to reasons other than the transformation nucleation-propagation hypothesis. The actual mechanism responsible for this instability is yet to be identified.

4. Numerical Simulations

This section revisits conclusions drawn by Shaw and Kyriakides from the unique consideration of localisation observed during tensile superelastic tests of NiTi alloys. Shaw et al have performed numerical simulation of localisation using two stress-strain responses [4]. The first one considered that the true stress-strain response maintained its stability during the plateau whereas the intermediate branch of the second one had a negative slope. The only argument supporting the second response was that it gave a larger initiation peak, in better agreement with experimental results. However, these conclusions were drawn from simulation performed neglecting thermomechanical coupling. In more recent simulations using only the second type of constitutive equations, it has been shown that this effect was very important [7].

Our simulation is restricted to isothermal cases and thus do not address the strong effect of thermomechanical coupling. The only purpose is to show that simulation using constitutive equations similar to those of the first model proposed by Shaw in [4] agrees well with experimental Lüders-like tensile tests, but also with compression tests for which homogeneous deformation was experimentally observed.

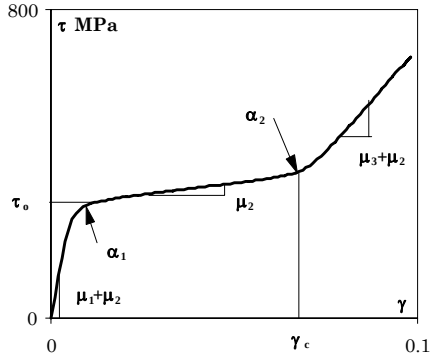

Figure 9: Definition of the parameters of the hyperelastic model in shear.

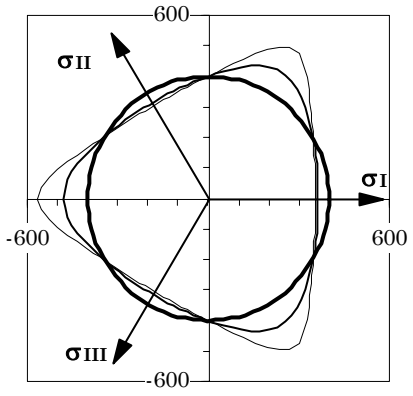

Figure 10: Transformation criteria plotted in the deviatoric stress plane.

Numerical results presented in this section use a simple hyperelastic scheme and account for large deformations. The set of constitutive equations were described in [15]. As an example, prediction of the model in a pure shear loading is illustrated with the stress-strain curve plotted in Figure 9. As evident in this figure, the model prediction is similar to the tri-linear stress-strain curve used by Shaw in [4], except that the three linear stages are connected by arcs. To run the simulation, the hyperelastic scheme requires the determination of 7 constitutive parameters:

- a transformation stress, *i.e.* τ_0,
- a transformation strain, *i.e.* γ_c,
- shear stress-strain moduli, for the initial, middle and final stages observed during superelasticity, *i.e.* $(\mu_1 + \mu_2)$, μ_2 and $(\mu_3 + \mu_2)$, respectively,
- a parameter which allows a continuous transition between the initial stage (very often considered as the elastic deformation of the austenite) and the middle stage associated with the transformation stage, *i.e.* α_1, and
- a parameter that characterizes gradual transition between the middle stage and the final stage (very often considered as the elastic deformation of martensite), *i.e.* α_2.

To account for the tension-compression asymmetry (Figures 1 and 2), the transformation criterion is not of Von-Mises type; this last one would be associated to the thick circle of Figure 10 which represents several transformation criteria plotted in the deviatoric stress plane. The thin curves are defined by three parameters, the shear transformation stress τ_0 (which is a linear function of the temperature, obeying a Clausius-Clapeyron relation) and two additional parameters γ_0 and n [16]. Such thin curves can easily be fitted from tension-compression and shear superelastic tests.

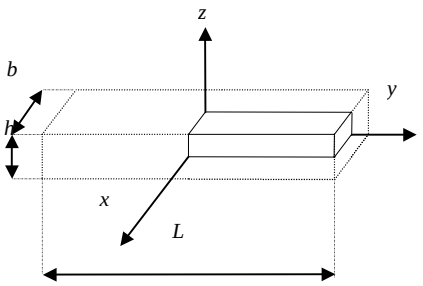

Figure 11: Geometry of the strip.

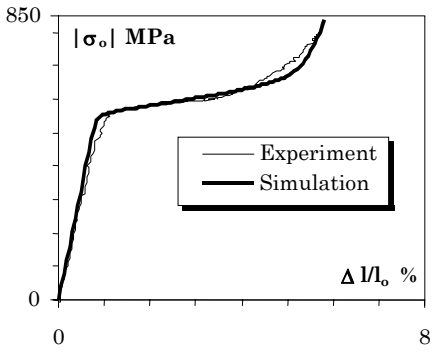

Figure 12: Modelling of the compression test

Models similar to Shaw's two models are obtained depending on the value of μ_2. Our simulation was performed with $\mu_2 = 245$ MPa, resulting in a positive slope for the true stress-strain function for shear, tension and compression stress state. Values of the other parameters together with the expressions of the curves defining the stress-strain response (Figure 9) and transformation criteria (Figure 10) are given in [15].

A strip of length $L = 50$ mm, thickness $h = 1$ mm and width b = 5 mm is considered, as depicted in Figure 11. Due to symmetry, only one eighth of the strip was meshed. Finite elements were 3D eight-node brick continuum elements. Results presented

bellow have been obtained with a gauge section of the meshed model consisting of 1 element through the half-thickness $h/2$, 8 elements through the half-width $b/2$ and 80 elements through the half-length $L/2$. The influence of the meshing was tested previously, showing that the as-described mesh was satisfactory for the accuracy of results and for non-costly computing [15].

To model uniaxial tension-compression loading, the following set of boundary conditions were prescribed to the strip schematised in Figure 11: $U_y(y = 0) = U_x(x = 0) = U_z\ (z = 0) = 0$ and $U_y\ (y = L/2)$ as a linear function of time. To induce Lüders-like deformation, a geometric imperfection was introduced in the strip by considering that the width of the strip was not perfectly constant but was a function of y:

$$b = b_0 + \Delta b \sin(\pi y/L) \qquad \text{with} \qquad b_0 = 5 \text{ mm}.$$

In this work, Δb was equal to 10^{-2} mm. It has been shown [15] that the simulated results were qualitatively similar for values of Δb ranging between 10^{-3} mm and 10^{-1} mm.

Figure 12 shows experimental and modelled engineering stress-strain curves for a compression test performed at 333 K. The simulation displays homogeneous deformation and the comparison between experiment and numerical simulation is fairly good.

Similar results are plotted in Figure 13 in the case of a tensile test performed at the same temperature. The force per unit of initial area is plotted as a function of the total length variation, both for experiment and numerical simulation. These two curves agree almost perfectly. Two strain measurements have been calculated from the results of the simulation. The first one, *i.e.* $\Delta l/l$, is based on the displacement of the point P_1 initially located at $x = z = 0$ and $y = 7.5$ mm, whereas the second one, *i.e.* $\Delta L/L$, is based on the displacement of the top of the strip ($y = 25$ mm). Figure 14 shows the comparison of experimental and simulated results concerning the localisation of the deformation. The simulated "global strain $\Delta L/L$" is plotted as function of the simulated "local strain $\Delta l/l$" in thick stroke. The thin curve represents the experimental global strain measurement ε% GM as function of the experimental local measurement ε% LM, as shown in Figure 3 during the loading OABCD.

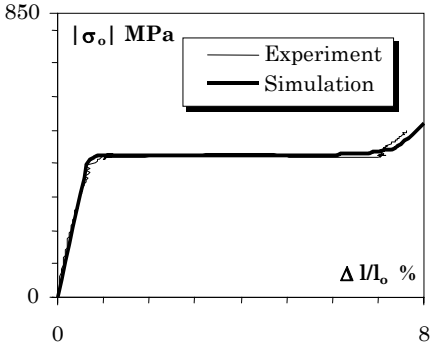

Figure 13: Modelling of the tensile test.

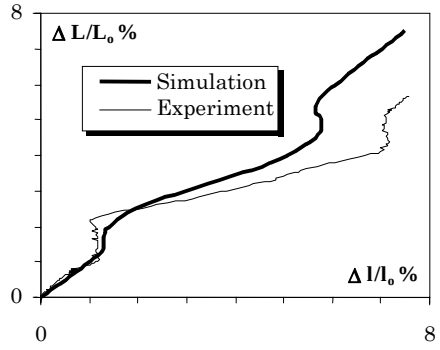

Figure 14: Modelling of the localisation during tensile test.

5. Conclusions

Several theories and constitutive equations have been proposed on the basis of experimental results of superelastic tensile tests exhibiting Lüders-like behaviour. This behaviour is not observed for other stress conditions like compression and shear, which negates the common association of the inhomogeneous deformation with phase transformation. Moreover, the present paper shows that inhomogeneous tensile tests together with homogeneous compression tests can be well simulated using usual stable constitutive equations.

REFERENCES

1. Miyazaki S., Imai T., Otsuka K., Suzuki Y., *Scripta Met*, **15** (1981), 853-856.
2. Shaw J.A. and Kyriakides S., *J. of Mech. Phys. Solids*, **43**, **8** (1995), 1243-1281.
3. Shaw J.A. and Kyriakides S., *Acta Materialia*, **45, 2** (1997), 683-700.
4. Shaw J.A. and Kyriakides S., *Int. J. of Plasticity*, **13, 10** (1998), 837-871.
5. McCormick P.G. , Liu Y., Miyazaki S., *Materials Science and Engineering, A*, **A167** (1993), 51-56.
6. Balandraud X., Ph. D thesis, University of Montpellier, France (2000).
7. Shaw J.A. , *Int. J. of Plasticity*, **16** (2000), 541-562.
8. Orgéas L., Favier D., *J. de Physique IV*, **5** C5 (1995), 605-611.
9. Orgéas L., Favier D., *Acta Materialia*, **46, 15**, (1998), 5579-5591.
10. Liu Yinong, Liu Yong, Van Humbeeck J., *J. Scripta Mat.*, **39, 8** (1998), 1047-1055.
11. Favier D., Guélin P., *Arch. Mech*, **37, 3** (1985), 201-219.
12. Liu Y., *Mat. Sci and Eng.*, **A271,** (1999), 506-508.
13. Miyazaki S., Otsuka K., Suzuki Y., *Scripta metal.*, **15** (1981), 287-292.
14. Liu Y., Liu Y., Van Humbeeck J., *Acta Materialia*, **47** (1999), 199-209.
15. Orgéas L., Favier D., Rio G., *Revue Européenne des Eléments Finis*, **7, 8** (1998), 111-136.
16. Orgéas L., Favier D., *Europ. Symp. On Mart. Transf. 2000*, Como, Italy, Sept. 2000, to be published in *J. de Physique IV*, (2001).